Time-of-Flight Signatures of Two Bosons in a Double Well

Analabha Roy and L.E. Reichl
Center for Complex Quantum Systems
and
Department of Physics
The University of Texas at Austin, Austin, Texas 78712

February 6, 2020

Abstract

We present analytical and numerical treatments for evaluating the time-of-flight momentum distribution for the stationary states of a two-boson system trapped in a quartic double-well potential, paying particular attention to the Tonks and noninteracting regimes. We find that the time-of-flight distributions can serve as a valuable tool in profiling the states of this system, which will be useful in understanding the chaotic dynamics of coherent quantum controlled excitations of trapped bosons.

1 Introduction

The study of ultracold boson systems in Optical Dipole Traps (ODT) such as Bose-Einstein condensates, have received considerable attention in academia in the last three decades [1] [2] [3] [4]. More recently, experiments involving number squeezed states of trapped alkali atoms have yielded promise [5]. New techniques, such as quantum tweezing [6] and quantum many-body culling [5], are being developed that can create mesoscopic two-boson systems out of ultra-cold atoms in optical traps. Theoretical studies demonstrate the possibility of number state generation by atomic culling as well [7]. Such a two-boson system can be subjected to a micrometer-scale double well by various means, ranging from small volume optical traps [5], to atom chips [8] [9]. An optical lattice of such double-wells can also be generated by two counter-propagating lasers of linearly polarized light with a known angle between their planes of polarization, and a transverse magnetic field to mix the two potentials [10]. If the on-site lattice depth is sufficiently deep then the tunneling between the sites can be neglected. Furthermore, if they are loaded homogeneously from a cold-atom system confined in an optical dipole trap by number squeezing, followed by adiabatically reducing the laser intensity so that the distribution in each site is

1

culled down to the subpoissonian regime (N=2 per site) [5], each double well system can be treated in isolation exactly as depicted in [11]. More recently (2009), number squeezing and subpoissonian distribution of atoms in each site in an optical lattice have been reported by Itah et al [12].

This system can then be excited to higher energies using stimulated Raman scattering. As we have shown [11], coherent population transfer from the ground state into one of the excited states can be achieved using time-modulated (ie pulsed) radiation pulses. If the time scale of the pulse modulation is sufficiently large, the Raman process is adiabatic (called Stimulated Raman Adiabatic Passage or STIRAP) [13]. The presence of avoided crossings contributed by resonating levels other than the ones that the radiation pulses connect have been predicted [11]. These avoided crossings in the Floquet eigenphases appear due to level repulsion caused by a loss of symmetry/degeneracy (actual crossings) [14], and affect the statistical properties of the spectra, bringing them close to that predicted by random matrix theory. These are connected with the dynamics of the underlying classical system, which undergo a transition from KAM tori to chaos in this region of the parameter space [14]. Thus, this system can be used to demonstrate the quantum effects of chaos, induced by the radiation, on multilevel transitions in a 2-boson system.

In the following sections, we evaluate the time of flight (tof) signatures of these wavefunctions, and discuss the extent to which they are useful in observing chaos. Section 2 details how the double well system was diagonalized and the eigenfunctions obtained. Section 3 discusses the nature of the time-of-flight signatures of the different states, and numerical results are shown in section 4. Concluding remarks are made in the final section.

2 The Eigensystem: Strongly Interacting and Single Particle Regimes

Our system consists of two alkali metal bosons confined to a double-well optical potential. The effective interaction between the bosons, in three dimensions, is obtained in the long wavelength approximation to be

$$u^{3d}(\mathbf{x}_1 - \mathbf{x}_2) = \frac{4\pi\hbar^2 a_s}{m}\delta(\mathbf{x}_1 - \mathbf{x}_2), \tag{1}$$

where $\hbar$ is Planck's constant, a_s is the s-wave scattering length and $\mathbf{x}_i = (x_i, y_i, z_i)$ is the displacement of the ith particle [15] [16]. The system can be confined in two spatial (radial) directions so that the essential dynamics occurs in the x - direction by the use of anisotropic magnetic traps with high aspect ratio [17] [18]. In that case, the other 2 dimensions can be integrated out [11] [17], yielding an effective 1-dimensional interaction

$$u(x_1 - x_2) = 4a_s\omega_s\hbar\delta(x_1 - x_2) \tag{2}$$

We will consider the case of two identical bosons confined to a quartic double well potential. We get the total Hamiltonian for the system to be

$$H = p_1^2 + p_2^2 + V_0(-2x_1^2 + x_1^4) + V_0(-2x_2^2 + x_2^4) + U_0\delta(x_1 - x_2). \qquad (3)$$

where p_i is the momentum of the ith particle (i= 1,2), x_i is the position of the ith particle along the x-axis, and V_0 determines the depth of the double well potential. We have used dimensionless expressions for all the degrees of freedom, as well as the system parameters, by introducing a characteristic length scale L_u. Thus, the actual Hamiltonian H' relates to the dimensionless Hamiltonian H as $H = \frac{H'}{E_u}$, where $E_u = \frac{\hbar^2}{2mL_u^2}$. Similarly, $U_0 = \frac{4a_s\omega_s\hbar}{E_u}$ and the time scales as $t = \frac{t'}{T_u}$ where $T_u = \frac{2mL_u^2}{\hbar}$. Fig. 1 shows a plot of the quartic double well $V(x) = V_0(-2x^2 + x^4)$ for well depth $V_0 = 7.2912229$.

The numerical diagonalization of the Hamiltonian in Eq. 3 is facilitated by a nonadaptive finite element method using the analytically obtained matrix elements of the Hamiltonian in a finite wave train basis of size $L = 3.5$ (in units of L_u),

$$\langle x_1, x_2 | n_1, n_2 \rangle^{(s)} = \frac{1}{\sqrt{2(1 + \delta_{n_1,n_2})}}[\langle x_1|n_1\rangle\langle x_2|n_2\rangle + \langle x_1|n_2\rangle\langle x_2|n_1\rangle]. \qquad (4)$$

Here,

$$\langle x|n\rangle = \frac{1}{\sqrt{L}}\sin\left[\frac{n\pi}{2}(\frac{x}{L} - 1)\right] \qquad (5)$$

within the range $-L \leq x \leq L$ and vanishes outside.

We will investigate the tof distributions in two regimes of the (V_0, U_0) parameter space of the double well system. Here, V_0 is the well depth, and U_0 the amplitude of the point contact pseudopotential in 1-dimension. The first regime, henceforth referred to as the 'strongly interacting regime' will consist of a very strongly repulsive system and a moderate well depth. We define the 'strongly interacting factor' for this system, γ, as

$$\gamma \equiv \frac{U_0}{E}. \qquad (6)$$

Here, E, the energy of the state, is a measure of the ability of the bosons to tunnel across from one well to another. When $\gamma \rightarrow \infty$, we reach the strongly interacting regime where the interaction completely dominates the system [19]. Figure 2 shows the evolution of the ground state of the system as γ is increased. The order parameter being plotted as a function of γ for the ground state is $p_i/\delta l$, where

$$p_i \equiv \delta l \int dx |\langle x, x|E_1\rangle|^2. \qquad (7)$$

Here, i is an index distinguishing different regimes of interest in the γ-space. Also, p_i is the total probability that the two particles will be together within
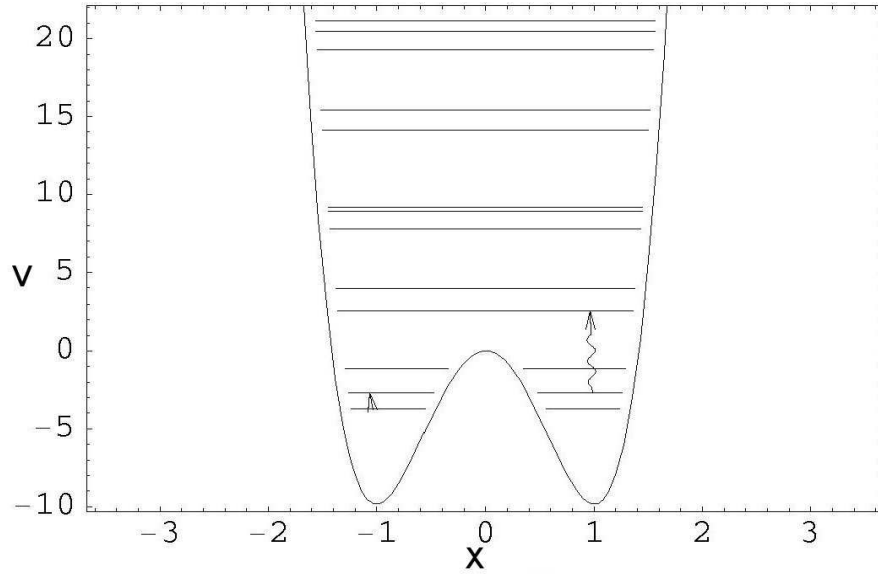
Figure 1: Plot of the double-well potential experienced by each boson for the single particle regime. The energy levels, $E_1 = -6.42262$, $E_2 = -5.68883$ and $E_4 = 0.640055$ of the interacting two-boson system (interaction strength $U_0 = -1.0$) are also sketched, with wavy arrows denoting the levels connected by the STIRAP pulses. Note the slightly detuned resonance between the $2 \leftrightarrow 4$ and the $4 \leftrightarrow 7$ levels where $E_7 = 6.96998$. Here, $V_0 = 7.2912229$.
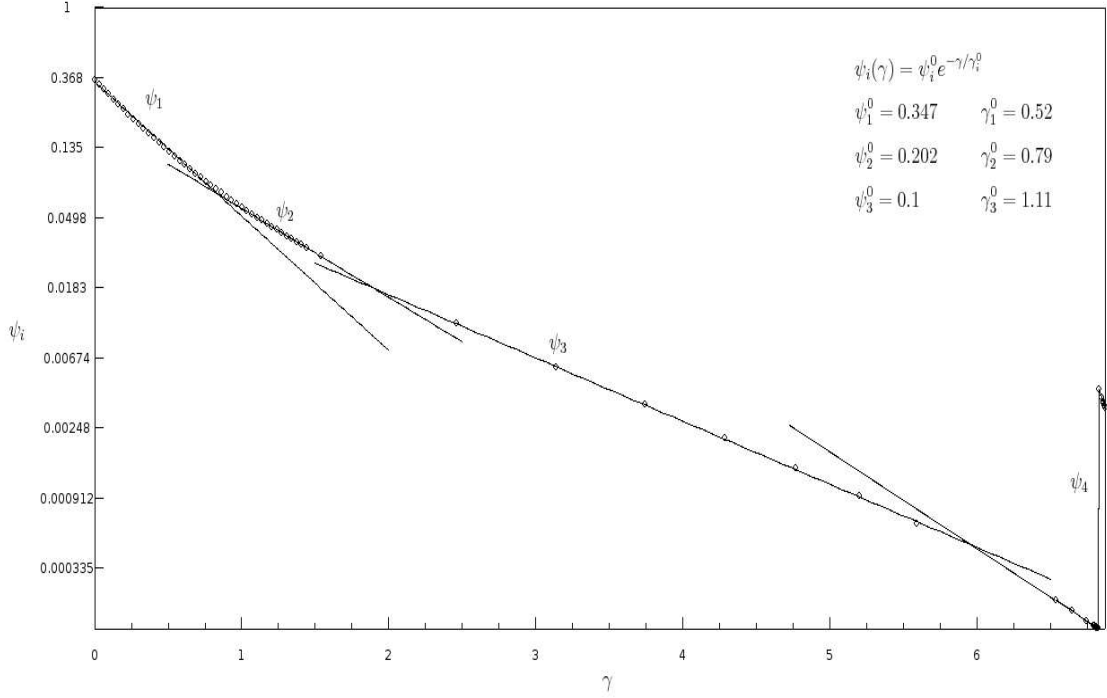
Figure 2: Semi-logarithmic plot of the one dimensional probability density $p_i/\delta l$ of two particles being within a rectangular strip of arbitrarily small width δl along the line $x_1 = x_2$. $p_i/\delta l$ is plotted as a function of the strongly interacting parameter γ for a constant $V_0 = 4.0$. The decay rate of the probability p_i changes sharply at 4 regions, labeled by the index i. The data points (indicated by circles) have been fitted to exponential decay rates at each region (indicated by lines).The legend provides the numerically fitted values of the decay rates γ_i^0. Note the discontinuous spike at $\gamma \sim 7$.

a rectangular strip along the line $x_1 = x_2$ and arbitrarily small width δl. As expected, it vanishes for large values of γ.

In this strongly interacting regime, the two particles have no probability of occupying the same position simultaneously. Thus, they act in a way that is similar to a Tonks gas [19]. The transition to this regime is not consistent, however. We note four distinct ranges of γ for which the decay rates of $p_i/\delta l$ are different. In the first three ranges, p_i seems to be decaying exponentially ie $(p_i/\delta l) = \left(p_i^0/\delta l\right) e^{-(\gamma/\gamma_i^0)}$ for $i = 1, 2, 3$. The data points have been fitted to exponents by the use of numerical nonlinear least-squares algorithms. The decay rate, characterized by γ_i^0, decreases sharply at $\gamma \sim 1, 2$ and 6. Near $\gamma \sim 7$, there is a sharp increase in p_i after which it continues to decrease. If we neglect the probability if it falls below $1/e$ of the maximum, then the 'strongly interacting regime' is achieved beyond $\gamma \sim 0.4$. In our case, we have chosen a γ of 5.20142 for our strongly interacting regime, placing the system in region 3 of Fig 2. The value of (V_0, U_0) chosen is $(4.0, 40.0)$.

The second regime, henceforth referred to as the 'single particle regime', will consist of a weakly attractive system and the well-depth as seen in [11]. Thus, the parameter values chosen are $(7.2912229, -1.0)$. The probability distributions of the ground state $|E_1\rangle$, as well as the excited states $|E_2\rangle$ and $|E_4\rangle$, given by Eqn 3 are shown in Figs 3.a through 3.c for the strongly interacting regime. Note that, as expected, there is virtually no probability that $x_1 = x_2$. The probability distributions of the first seven quantum energy states of the system in the single particle regime are shown in Figs. 4.a through 4.g. Note the plots of the ground state, $|E_1\rangle$, third excited state, $|E_4\rangle$, and sixth excited state $|E_7\rangle$. The dynamics of the system, when driven by sequential pulses whose energies are tuned to transitions between these states, show the effects of dynamical chaos through level-repulsion in the Floquet eigenphases [11]. A crossing through the level-repelling region can be avoided if the radiation pulses are applied adiabatically, producing a chaos assisted passage as detailed in [11].

3   Time of Flight Images

The normalized first order correlation function of a single double well is a measurement of the atomic density $n(x)$. Such correlations can be measured following a STIRAP transition by the time-of-flight (TOF) technique in which the trapped atoms are released sufficiently quickly that the diabatic approximation in quantum mechanics can be applied. The atoms then expand ballistically until they reach a detection plate. If the plate is far enough from the double well system that the far-field approximation can be used, then the Green's Function for the system can be simplified and the time translation reduced to a simple Fourier Transform. If the 'detector plane' coordinates are denoted by unprimed variables $[x_1, x_2, t]$ and the double -well coordinates by primed variables $[x_1', x_2', t]$ for a 2-particle system after all the external fields and traps have been diabatically switched off, and the interactions between the atoms rendered negligible by tuning a homogeneous magnetic field close to the Feshbac
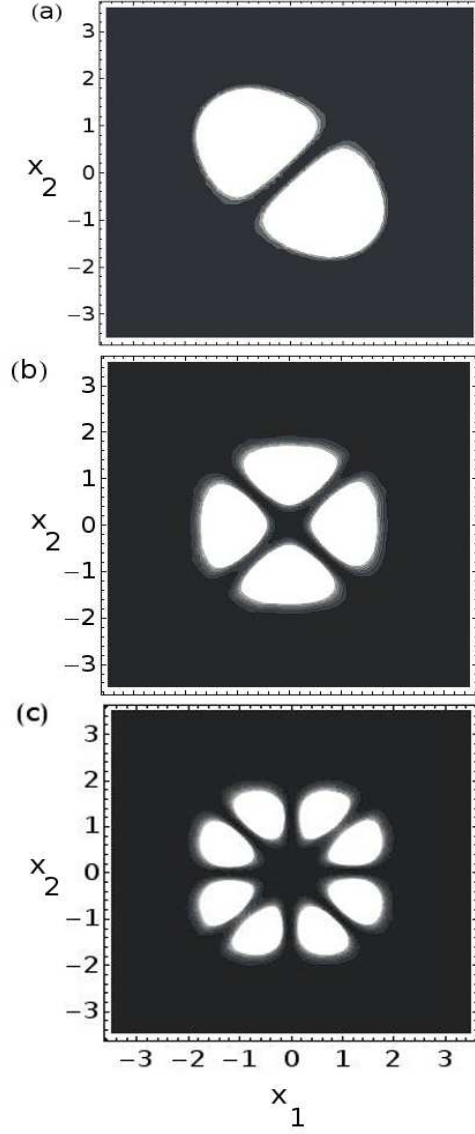
Figure 3: Plots of energy eigenfunctions for the two interacting bosons in a double well potential in the strongly interacting regime. Figures (a) through (c) are contour plots of the probability density $|\langle x_1, x_2|E_1\rangle|^2$, $|\langle x_1, x_2|E_2\rangle|^2$ and $|\langle x_1, x_2|E_4\rangle|^2$ respectively. The probabilities are plotted as functions of x_1 and x_2. All units for all figures are dimensionless
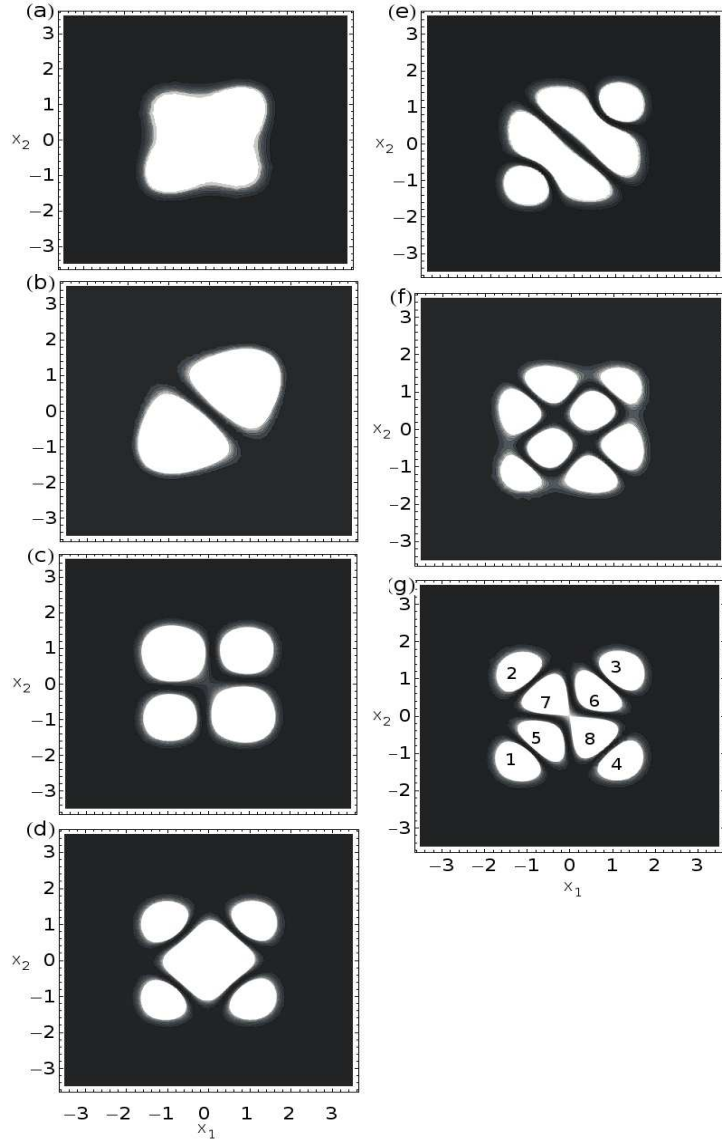
Figure 4: Plots of energy eigenfunctions for the two interacting bosons in a double well potential in the single particle regime. All units are dimensionless. Figures (a) through (f) are contour plots of the probability density $|\langle x_1, x_2 | E_1 \rangle|^2$ through $|\langle x_1, x_2 | E_6 \rangle|^2$ respectively. Figure (g) is a contour plot of the probability density $|\langle x_1, x_2 | E_7 \rangle|^2$. The peaks in the probability are numbered. The probabilities are plotted as functions of x_1 and x_2. All units for all figures are dimensionless

8

resonance that adds an attractive amplitude to the normally repulsive point contact pseudopotential [20] [16]. The system then evolves ballistically in free space.

The Green's Function or Propagator $G(\mathbf{x}, t; \mathbf{x}', t')$ is defined by

$$\Psi(\mathbf{x}, t) = \int d^2 x \; G(\mathbf{x}, t; \mathbf{x}', t') \Psi(\mathbf{x}', t'), \tag{8}$$

where $\mathbf{x} = [x_1, x_2]$, and $\Psi(\mathbf{x}, t)$ is the wavefunction, with similar expressions for the primed coordinates. For free space, the relevant 1-dimensional Schrödinger equation for 2-particles is

$$\left[H - i\frac{\partial}{\partial t} \right] \Psi(\mathbf{x}, t) = 0,$$

$$H = - \left[\frac{\partial^2}{\partial x_1^2} + \frac{\partial^2}{\partial x_2^2} \right]. \tag{9}$$

Thus, the Green's function [21] will be the solution to

$$\left[H - i\frac{\partial}{\partial t} \right] G(\mathbf{x}, t; \mathbf{x}', t') = \delta(\mathbf{x} - \mathbf{x}')\delta(t - t'). \tag{10}$$

The solution to Eqn 10 in free space is

$$G(\mathbf{x}, t; \mathbf{x}', t') = \frac{\sqrt{-i}}{L} \exp\left[i\pi |\frac{\mathbf{x} - \mathbf{x}'}{L}|^2 \right]. \tag{11}$$

Here, the ballistic de-Broglie equation,

$$L^2 = 4\pi\tau, \tag{12}$$

provides the relation between the detector-system separation L and the time-of-flight $\tau = (t - t')$.

Now, consider such a two particle system localized at a site j. The wavefunction is localized about $\mathbf{x}'_j = \left[x'_j, x'_j \right]$ and can be written in the form $\Psi(\mathbf{x}' - \mathbf{x}'_j)$. We now use Eqns 11 and 12 on Eqn 8, and apply the shift theorem for Fourier transforms [22] [23] to get

$$\Psi(x, \tau) = \sqrt{\frac{-i}{4\pi\tau}} \exp\left[i\frac{1}{2\tau} \left(\frac{|\mathbf{x}|^2}{2} + \mathbf{x} \bullet \mathbf{x}'_j \right) \right] F\left[\Psi(\mathbf{x}')\right]_{\mathbf{u} = \frac{\mathbf{x}}{4\pi\tau}}, \tag{13}$$

where the primed coordinates refer to the double well system, the unprimed coordinates refer to the detector, and $F\left[\Psi(\mathbf{x}')\right]_{\mathbf{u}}$ is the Fourier transform

$$F\left[\Psi(\mathbf{x}')\right]_{\mathbf{u}} \equiv \frac{1}{2\pi} \int d^2 x' \Psi(\mathbf{x}') e^{i\mathbf{u} \bullet \mathbf{x}'}. \tag{14}$$

In the equation above, $\mathbf{u} = [u_1, u_2]$ is the momentum space vector. For a large collection of such systems, each in the desired pure state, the measured TOF is

simply the probability obtained from Eqn 13 times the number of such double wells N (which we shall subsequently drop off as an appropriately adjusted overall normalization).

$$n(\mathbf{x}) = N \frac{1}{4\pi\tau} |F\left[\Psi(\mathbf{x}')\right]_{\mathbf{u}=\frac{\mathbf{x}}{4\pi\tau}}|^2. \tag{15}$$

We note that there are noticeable differences in the symmetries of the two states $|E_4\rangle$ and $|E_7\rangle$ (refer to Figs 4). The distinctly resolved peaks in each wavefunction (labeled 1 through 8 for $|E_7\rangle$) can be approximated by elliptical Gaussian functions. Thus, the wavefunction can be represented by a two-dimensional function as follows:

$$\Psi(x_1', x_2') = \sum_{i=1}^{R} a_i G\left(x_1', x_1^i, \alpha_1^i\right) G\left(x_2', x_2^i, \alpha_2^i\right), \tag{16}$$

where

$$G(x, x^i, \alpha) = \left(\frac{2\alpha}{\pi}\right)^{1/4} e^{-\alpha\left(x-x^i\right)^2}. \tag{17}$$

Here, R is the number of peaks (8 for $|E_7\rangle$). Also, we have rotated our coordinate system to the axes of symmetry (by 45 degrees) of $|E_7\rangle$. Using the well-known relation for the Fourier transform of a Gaussian applied to Eqns 15 and 16, we get (sans any overall normalizations),

$$n(x_1, x_2) = |\sum_{j=1}^{R} a_j \left(\frac{1}{4\pi^2\alpha_1^j\alpha_2^j}\right)^{1/4} e^{i\frac{x_1 x_1^j + x_2 x_2^j}{4\pi\tau}} e^{-\frac{x_1^2}{16\pi^2\alpha_1^j\tau^2}} e^{-\frac{x_2^2}{16\pi^2\alpha_2^j\tau^2}}|^2. \tag{18}$$

We rewrite this as

$$n(x_1, x_2) = |\sum_{j=1}^{R} r_j(x_1, x_2) e^{ik_j x_1}|^2,$$

$$r_j(x_1, x_2) = a_j \left(\frac{1}{4\pi^2\alpha_1^j\alpha_2^j}\right)^{1/4} e^{i\frac{x_2 x_2^j}{4\pi\tau}} e^{-\frac{x_1^2}{16\pi^2\alpha_1^j\tau^2}} e^{-\frac{x_2^2}{16\pi^2\alpha_2^j\tau^2}},$$

$$k_j = \frac{x_1^j}{4\pi\tau}. \tag{19}$$

The expression above can be simplified to

$$n(x_1, x_2) = \sum_{j=1}^{R} |r_j(x_1, x_2)|^2 + \sum_{\langle i,j \rangle} 2r_i^*(x_1, x_2) r_j(x_1, x_2)| \cos\left(k_j - k_i\right)x|. \tag{20}$$

In order to get the density functional $n(x)$, we integrate out the x_2 (symmetries guarantee that the result will be the same if we integrate x_1 instead) and get

$$n(x) = \sum_{j=1}^{R} r_j^2(x) + \sum_{\langle i,j \rangle} 2r_{ij}^2(x)| \cos\left(k_j - k_i\right)x|, \tag{21}$$

10

where $\langle i,j \rangle$ are distinct (ie $i \neq j$) combination pairs of peaks. In the equation above, integrating x_2 by Gaussian integral methods leaves out a Gaussian dependencies in x of r_j and r_{ij} (the subscripts for x have been dropped). Thus,

$$r_j^2(x) = \tau a_j^2 \sqrt{\frac{4\pi}{\alpha_1^j}} e^{-\frac{x^2}{16\pi^2 \alpha_1^j \tau^2}},$$

$$r_{ij}^2(x) = 2\tau a_i a_j \left(\frac{1}{\alpha_1^i \alpha_1^j \alpha_2^i \alpha_2^j} \right)^{\frac{1}{4}} \sqrt{\pi \alpha_2^{ij}} e^{-\frac{\alpha_2^{ij}(x_2^j - x_2^i)^2}{4}} e^{-\frac{x^2}{16\pi^2 \alpha_1^{ij} \tau^2}}, \qquad (22)$$

where we have defined

$$\frac{1}{\alpha^{ij}} \equiv \frac{1}{\alpha^i} + \frac{1}{\alpha^j}. \qquad (23)$$

From the plot of $|E_7\rangle$ for the single particle regime (see Fig 4), we notice that there are only three distinct kinds of peaks (labeled 1, 5 and 8). Thus there are three pairs whose k's are unequal viz. $\langle 1,5 \rangle$ and $\langle 1,8 \rangle$ and $\langle 5,8 \rangle$. All other terms are absorbed into the perfect square terms in Eqn 21. Each such term is a Gaussian centered at $x = 0$ with varying widths. If we look at values of x sufficiently far from the center of the detector plate, those terms drop off quickly, leaving just the three oscillatory terms. This signal will be distinct from that obtained from the TOF of state $|E_4\rangle$, which has only 2 such term (only 2 distinct kinds of peaks). If the time-of-flight τ is chosen so that the values of $k_j - k_i$ are small, then the signal will look like an amplitude modulated sinusoid.

4   Time-of-Flight: Numerical Plots

This section will detail the procedure for obtaining numerical plots of the tof distributions of the eigenstates of the double well system. The two boson problem in a double well is diagonalized as detailed in section 2 and [11]. Thus, the eigenfunctions are obtained as linear superpositions of the eigenfunctions of two bosons in a box of appropriately chosen length L, ie

$$\langle x_1, x_2 | n_1, n_2 \rangle^{(s)} = \frac{1}{\sqrt{2(1 + \delta_{n_1, n_2})}} [\langle x_1 | n_1 \rangle \langle x_2 | n_2 \rangle + \langle x_1 | n_2 \rangle \langle x_2 | n_1 \rangle],$$

$$\langle x | n \rangle = \frac{1}{\sqrt{L}} \sin \left[\frac{n\pi}{2} \left(\frac{x}{L} - 1 \right) \right], \qquad (24)$$

if $|x_i| < L$, and 0 otherwise. Thus, the final solution to an eigenfunction $|E_n\rangle$ of the double well will be a linear superposition of the 'finite wave train' functions defined above, ie

$$\langle x_1, x_2 | E_n \rangle = \sum_{[n_1, n_2]=[1,1]}^{[N,N]} C_{E_j}^{[n_1, n_2]} \langle x_1, x_2 | n_1, n_2 \rangle^{(s)}, \qquad (25)$$

11

where the $C_{E_j}^{[n_1,n_2]}$ are obtained numerically using the nonadaptive finite element method. This result can then be substituted into Eqn 15 to get

$$n(x_1, x_2) = N \frac{1}{4\pi\tau} | \sum_{[n_1,n_2]=[1,1]}^{[N,N]} C_{E_j}^{[n_1,n_2]} F\left[\langle x_1', x_2'|n_1,n_2\rangle^{(s)}\right]_{[u_1,u_2]=\frac{[x_1,x_2]}{4\pi\tau}} |^2.$$

$$(26)$$

Using the linearity of Fourier Transforms and Eqn 24, we get

$$F\left[\langle x_1', x_2'|n_1,n_2\rangle^{(s)}\right]_{\mathbf{u}} = \frac{1}{\sqrt{2(1+\delta_{n_1,n_2})}}$$
$$(F[\langle x_1|n_1\rangle]_{u_1} F[\langle x_2|n_2\rangle]_{u_2} + F[\langle x_1|n_2\rangle]_{u_1} F[\langle x_2|n_1\rangle]_{u_2}). \quad (27)$$

The Fourier transform of the finite wave train ($\langle x|n \rangle$ in Eqn 24) can be calculated using Gaussian integrations [24] to yield

$$F[\langle x'|n\rangle]_u = \frac{1}{\sqrt{2L\pi}} \frac{1}{\left(\frac{n^2\pi^2}{4L^2} - u^2\right)} \left[2u \sin\frac{n\pi}{2} - \frac{n\pi}{L}\sin Lu\right], \quad (28)$$

where u is the momentum space vector. Thus, by plugging Eqn 28 into Eqn 27, and that into Eqn 26, the tof distribution $n(x_1, x_2)$ can be obtained, the final density distribution is the density functional average of this result viz.

$$n(x) = \int dx' n(x, x'). \quad (29)$$

Thus, a numerical expression for Eqn 15 was obtained for two degrees of freedom x_1 and x_2, and the density functional $n(x)$ determined by integrating out one of the coordinates by adaptive Gauss-Kronrod quadrature.

Numerical results for the tof distributions of the eigenstates of the double well for the strongly interacting and single particle regimes are shown in Figs 5 and 6 respectively. The distributions are shown for tof $\tau = 10^5$ units of T_u. All the dynamics is essentially independent of the characteristic length scale L_u (the actual position of the well minima). For practical reasons, we choose an L_u of 50 nm [11]. Consequently, with a Rubidium-85 atomic mass of 85.4678 $gmol^{-1}$, we get a T_u of about 6.7 μs, which makes τ to be 0.67 seconds. Using Eqn 12, we get a detector distance of about 2.2 cm.

Figures 5(a) through (c) show the tof distributions of the states $|E_1\rangle$, $|E_2\rangle$, and $|E_4\rangle$ respectively for the strongly interacting gas detailed in section 1. Note that the the momentum distribution of $|E_1\rangle$, closely approximates the Heavyside function that is characteristic of the momentum distribution of a Tonks gas [19] (barring the lack of any occupancy at zero momentum, which is forbidden in this case due to a nonzero value of the ground state energy E_1).

Figures 6(a) through (c) show the tof distributions of the states $|E_1\rangle$, $|E_4\rangle$, and $|E_7\rangle$ respectively in the single particle regime detailed in section 1. Note that, as predicted by the calculations in section 3, the number of distinct oscillations in each distribution correspond to the number of distinct pairs of peaks

seen in the wavefunctions. Thus, each state generates a particular signature in the tof. Since the transitions to $|E_4\rangle$ and $|E_7\rangle$ are caused by crossing or avoiding a chaos assisted adiabatic passage, the amplitude modulation in the tof differentiates between the two outcomes. In case there is an incoherent excitation, there will be large numbers of overlapping or closely spaced peaks and the oscillations will constructively interfere everywhere, thus distinguishing the resultant signal from one obtained by the TOF of a coherent excitation. Thus, the influence (or lack thereof) of chaos in the underlying classical dynamics can be indirectly inferred by the one extra oscillation in Fig 6(c) compared to Fig 6(b).

Time of flight fluorescence methods for profiling the wavefunction, such as measuring the momentum distribution by interrupting the particle flow with counter-propagating laser beams and then measuring fluorescence as a function of time (time of flight absorption) [25] [26], will have high signal to noise ratio (compared to absorption) [5]. Single shot fluorescence images should duplicate the profile shown in Figs 6(a)-(c) for a double well system produced by optical lattices. For a single magnetically confined double well, repeated measurements of position by the means of atom detectors, or by performing scanning tunneling microscopy on an appropriate substrate where the atoms are allowed to deposit after their tof expansion, should reproduce the required results.

5 Conclusions

We have obtained and analyzed the time-of-flight images of a two-boson system subjected to optical double well potentials. The tof plots help in distinguishing the different outcomes of STIRAP excitations of such systems, depending on the time scales of the driving radiation pulses. The presence of chaos in these dynamics affect the outcome and influence the pattern that will be seen on the detector as extra oscillations in the spatial variation of fluorescense.These oscillations can be resolved by choosing an appropriately high value of τ which reduces the frequencies. The momentum probability distributions of the tof do not provide enough information to uniquely profile the original wavefunction spatially, since two neighboring states with opposite parities will provide nearly the same tof distribution. However, quantum control methods like STIRAP can be tuned to forbid those transitions, making tof a valuable tool in profiling the final states of quantum controlled excitations in cold atom systems.
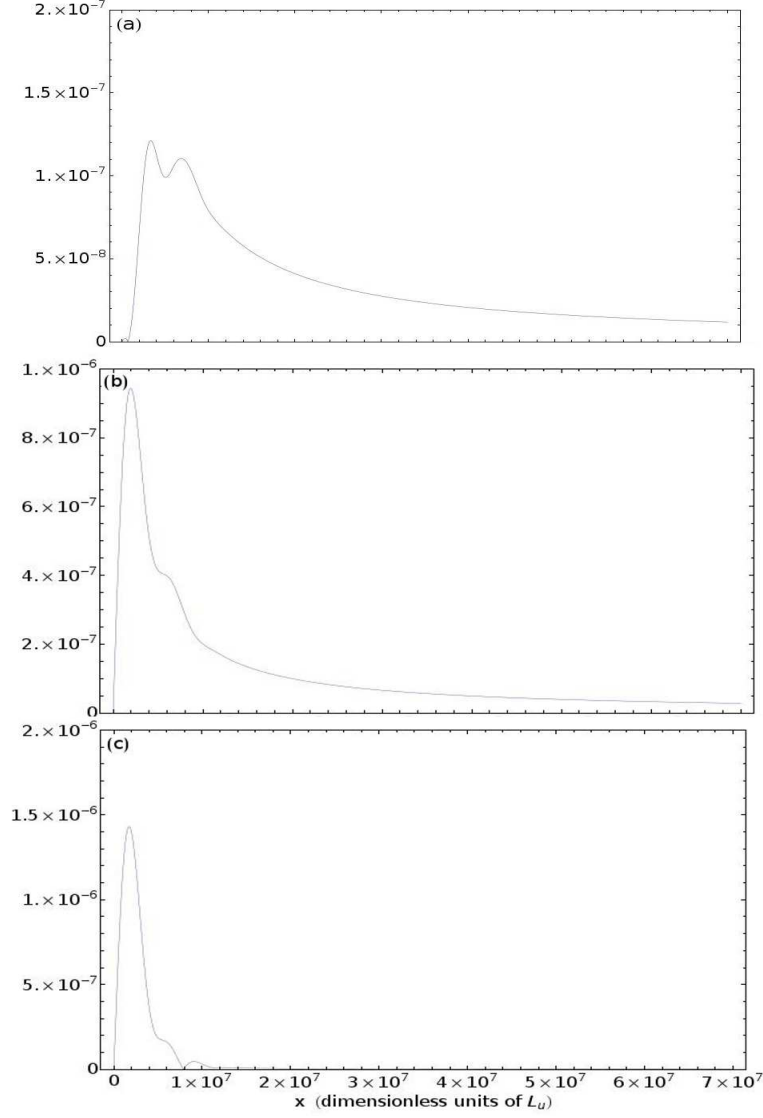
6 Acknowledgments

Figure 5: Figures (a) through (c) are plots of the one-dimensional time-of-flight distributions for the double-well eigenstates $|E_1\rangle$, $|E_4\rangle$ and $|E_7\rangle$ respectively in the strongly interacting regime. The distributions are symmetric about $x = 0$, so only the positive half is shown. The number density $n(x)$ in the ordinate is for 10^6 double wells after a time of flight $\tau = 10^5$ (in units of T_u). The abscissa is shown in dimensionless units of L_u.
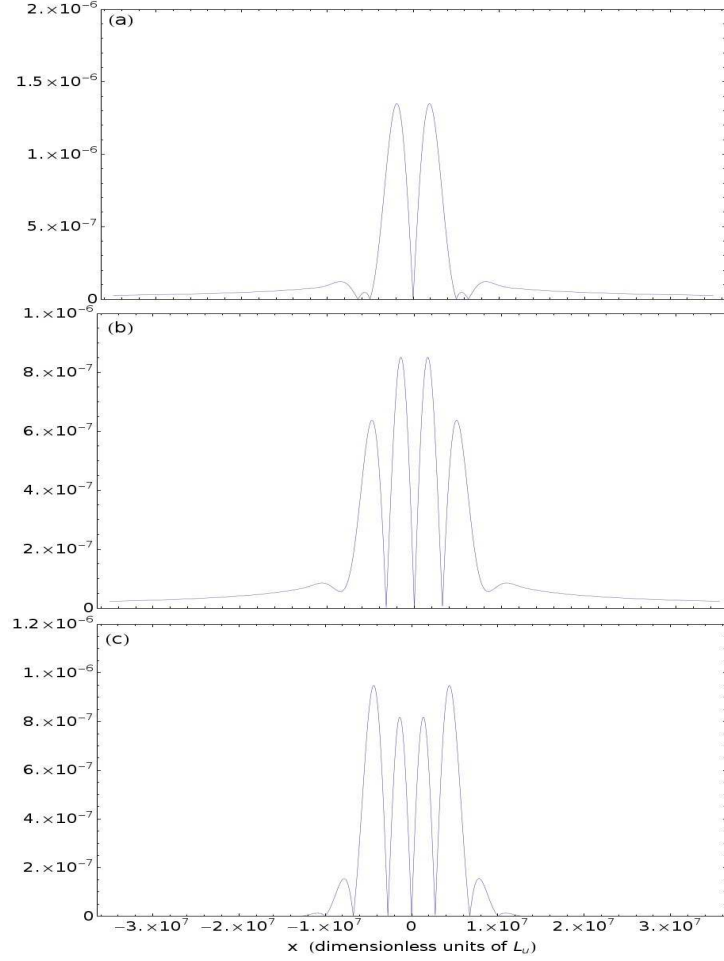
Figure 6: Figures (a) through (c) are plots of the time-of-flight distributions for the double-well eigenstates $|E_1\rangle$, $|E_4\rangle$ and $|E_7\rangle$ respectively in the single particle regime. The number density $n(x)$ in the ordinate is for 10^6 double wells after a time of flight $\tau = 10^5$ (in units of T_u). The abscissa is shown in dimensionless units of L_u.

16

References

[1] C. Monroe, W. Swann, H. Robinson, and C. Wieman. Very cold trapped atoms in a vapor cell. *Phys. Rev. Lett.*, 65(13):1571–1574, Sep 1990.

[2] M.H. Anderson, J.R. Ensher, M.R. Matthews, C.E. Weiman, and E.A. Cornell. Observation of Bose-Einstein Condensation in a Dilute Atomic Vapor. *Science*, 269:198–201, July 1995.

[3] Wolfgang Ketterle, Kendall B. Davis, Michael A. Joffe, Alex Martin, and David E. Pritchard. High densities of cold atoms in a dark spontaneous-force optical trap. *Phys. Rev. Lett.*, 70(15):2253–2256, Apr 1993.

[4] K. B. Davis, M. O. Mewes, M. R. Andrews, N. J. van Druten, D. S. Durfee, D. M. Kurn, and W. Ketterle. Bose-Einstein Condensation in a gas of Sodium atoms. *Phys. Rev. Lett.*, 75(22):3969–3973, Nov 1995.

[5] C.-S. Chuu, F. Schreck, T. P. Meyrath, J. L. Hanssen, G. N. Price, and M. G. Raizen. Direct Observation of Sub-Poissonian Number Statistics in a Degenerate Bose Gas. *Phys. Rev. Lett.*, 95(26):260403, Dec 2005.

[6] Roberto B. Diener, Biao Wu, Mark G. Raizen, and Qian Niu. Quantum tweezer for atoms. *Phys. Rev. Lett.*, 89(7):070401, Jul 2002.

[7] A. M. Dudarev, M. G. Raizen, and Qian Niu. Quantum Many-Body Culling: Production of a Definite Number of Ground-State Atoms in a Bose-Einstein Condensate. *Physical Review Letters*, 98(6):063001, 2007.

[8] Schumm, T., Kruger, P., Hofferberth, S., Lesanovsky, I., Wildermuth, S., Groth, S., Bar-Joseph, I., Andersson, L., Schmiedmayer, and J. A Double Well Interferometer on an Atom Chip. *Quantum Information Processing*, 5(6):537–558, December 2006.

[9] T. Schumm, S. Hofferberth, L. M. Andersson, S. Wildermuth, S. Groth, I. Bar-Joseph, J. Schmiedmayer, and P. Kruger. *Nature Physics*, 1(1):57–62, 2005.

[10] Ivan H. Deutsch and Poul S. Jessen. Quantum-state control in optical lattices. *Phys. Rev. A*, 57(3):1972–1986, Mar 1998.

[11] Analabha Roy and L. E. Reichl. Coherent Control of Trapped Bosons. *Physical Review A (Atomic, Molecular, and Optical Physics)*, 77(3):033418, 2008.

[12] A. Itah, H. Veksler, O. Lahav, A. Blumkin, C. Moreno, C. Gordon, and J. Steinhauer. Direct observation of number squeezing in an optical lattice. Can be viewed at `http://arxiv.org/abs/0903.3282`, Mar 2009.

[13] Nikolay V. Vitanov, Thomas Halfmann, Bruce W. Shore, and Klaas Bergmann. Laser-induced population transfer by adiabatic passage techniques. *Annu. Rev. Phys. Chem.*, 52(763), 2001.

[14] L.E. Reichl. *The Transition to Chaos: Conservative Classical Systems and Quantum Manifestations*. Springer Verlag, Berlin, 2 edition, 2004.

[15] H.J. Metcalf and P. van der Straten. *Laser Cooling and Trapping*. Springer Verlag, New York, 1999.

[16] C.J. Pethick and H. Smith. *Bose-Einstein Condensation in Dilute Gases*. Cambridge University Press, 2002.

[17] M. Olshanii. Atomic Scattering in the Presence of an External Confinement and a Gas of Impenetrable Bosons. *Phys. Rev. Lett.*, 81(5):938–941, Aug 1998.

[18] D. S. Petrov, G. V. Shlyapnikov, and J. T. M. Walraven. Regimes of Quantum Degeneracy in Trapped 1D Gases. *Phys. Rev. Lett.*, 85(18):3745–3749, Oct 2000.

[19] Belen Paredes, Artur Widera, Valentin Murg, Olaf Mandel, Simon Folling, Ignacio Cirac, Gora V. Shlyapnikov, Theodor W. Hansch, and Immanuel Bloch. *Nature*, 429(6989):277–281, 2004.

[20] H. Feshbach. *Ann. Phys.*, 19(287), 1962.

[21] J.J. Sakurai. *Modern Quantum Mechanics*. Addison-Wesley, revised edition, 1999.

[22] Joseph W. Goodman. *Introduction to Fourier Optics*. Roberts and Company, third edition, 2005.

[23] John Grondalski, Paul Alsing, and Ivan Deutsch. Spatial correlation diagnostics for atoms in optical lattices. *Opt. Express*, 5(11):249–261, 1999.

[24] G B Arfken and H J Weber. *Mathematical Methods for Physicists*. Harcourt Academic Press, 5th edition, 2001.

[25] Paul D. Lett, Richard N. Watts, Christoph I. Westbrook, William D. Phillips, Phillip L. Gould, and Harold J. Metcalf. Observation of Atoms Laser Cooled below the Doppler Limit. *Phys. Rev. Lett.*, 61(2):169–172, Jul 1988.

[26] Georg Raithel. More about optical lattices. Available as `http://cold-atoms.physics.lsa.umich.edu/projects/lattice/latticeindex.html`.